ELSEVIER

International Journal of Pharmaceutics 189 (1999) 19–28

international journal of pharmaceutics

www.elsevier.com/locate/ijpharm

Measuring water distribution in extrudates using magnetic resonance imaging (MRI)

G. Tomer [a], M.D. Mantle [b], L.F. Gladden [b], J.M. Newton [a,*]

[a] *Department of Pharmaceutics, The School of Pharmacy, University of London, 29–39 Brunswick Square, London WC1N 1AX, UK*

[b] *Magnetic Resonance Research Centre, Department of Chemical Engineering, University of Cambridge, Pembroke Street, Cambridge CB2 3RA, UK*

Received 12 February 1999; received in revised form 2 July 1999; accepted 8 July 1999

Abstract

Magnetic resonance imaging (MRI) has been applied to the evaluation of the distribution of water in extrudates produced by extruding pastes. Two model drugs similar in chemical structure were mixed with microcrystalline cellulose (MCC) and with two different amounts of water and extruded at two different extrusion speeds using a ram extruder. Extrudates were collected during the steady-state stage of the extrusion profile and were analysed for the water distribution using MRI. The percolation threshold for each sample was calculated to evaluate the degree of water structure within the sample. The water distribution inside the extrudates was surprisingly uniform. The extrudates produced using the faster extrusion speed had a significant lower percolation threshold, which suggests the existence of a greater water structure in the extrudates. A significant correlation was found between the percolation threshold and the extrusion force, which had been used to provide the extrudates.

Keywords: Extrusion; Water movement; Magnetic resonance imaging (MRI); Water mapping; Percolation

1. Introduction

The extrusion process is used in several different industries to manufacture a wide range of products, such as: rubber, plastic, explosives, foods etc. The pharmaceutical industry uses this process as the first phase of a bi-stage process for the production of pellets, by placing the extrudates on a spheroniser's rotating plate which chops and rounds the extrudates to spherical pellets. The process is claimed to produce uniform sized pellets of smooth surface, which makes the coating process more effective, to give a reproducible and uniform controlled release drug profile. Although this process has been known for many years, rheological evaluation of pastes is difficult because it involves the application of stresses that can induce changes in the paste's

* Corresponding author. Tel.: +44-171-7535869; fax: +44-171-7535942.

E-mail address: newton@cua.ulsop.ac.uk (J.M. Newton)

0378-5173/99/$ - see front matter
PII: S0378-5173(99)00233-1

consistency due to the movement of fluid within the sample being measured. The extrusion process involves a major contribution from the liquid component in the system, normally water. The liquid acts as a lubricant, hence at higher water contents, the force required to push the wet mass through the die is lower. In addition, an increased water content decreases the plasticity, reducing the force necessary to extrude the paste (Harrison et al., 1985). It is known that water moves at a higher rate than the solids, usually resulting in extrudates which are wetter than the original wet mass (Fielden et al., 1989; Baert et al., 1992; Tomer and Newton, 1999). Due to the high pressures involved, steel equipment is required which makes it difficult to observe what happens to the liquid during the process. Fielden et al. (1989), Baert et al. (1992), Harrison (1982) and Tomer and Newton (1999) examined the extent of movement of water during the extrusion process by evaluation of the water content of extrudates. Burbidge et al. (1995) examined the water migration while consolidating wet ceramic pastes using a membrane filter instead of a die. The existence of convergence patterns in the extrusion of pastes has been observed (Harrison et al., 1984; Fielden et al., 1989). Thus, the paste converges into the restricted cross-section to flow through the die. Here the flow of such systems has been shown to be non-Newtonian (Harrison et al., 1987; Raines et al., 1990; Chohan and Newton, 1996). It has been suggested by Benbow et al. (1987) for ceramic pastes, that the type of flow through the die is plug flow, with a layer of water rich phase at the wall of the die. If this is the case for the pharmaceutical materials, one would anticipate a variation in water content across the extrudate with an outer layer being wetter than the centre. There is a need therefore to evaluate the water distribution across the extrudate to test this hypothesis. A technique, which has the potential to achieve this, is magnetic resonance imaging (MRI).

MRI is extensively used for medical imaging. It has been used also for mapping of liquids in solid objects in many different fields of research. The advantages of using MRI are:

1. It is a non-destructive and non-invasive method. Hence, MRI does not require slicing of the sample which could induce changes to the water distribution.
2. It can be selective to a certain region of the sample.
3. It can give the relative concentration as a function of spatial location, providing that the relaxation characteristics are uniform throughout the sample or are known and can therefore be corrected for (Hyde et al., 1995a).

Borgia et al. (1994) used MRI to look at the distribution of residual water in dolomite cores after saturating them with oil. Rajabi-Siahboomi et al. (1994) looked at the swelling of hydrating HPMC tablets using this MRI approach. Kojima et al. (1998) looked at the differences between swelling of micronized low-substituted hydroxypropylcellulose tablets and swelling of HPC and HPMC tablets. They showed that MRI, in this case, was sensitive enough to distinguish between the gel layer formed and the core of the tablet. Hyde et al. (1995b) examined the effect of a presence of a drug on properties such as buffer uptake kinetics, drug distribution in the polymer and other properties. Gotz and Buggisch (1993) used MRI to examine water movement in the extrusion barrel of a ram extruder while extruding a ceramic paste, glass spheres and glass powder. Tomer et al. (1999) used MRI to investigate water distribution occurring inside the extrusion barrel by analysing plugs from different stages of the extrusion process. MRI has also been used to visualise flow. Sinton and Chow (1990) studied the flow of solid-rocket motor propellant. Gullberg et al. (1990) looked at flow of blood through blood vessels that are unreachable with standard visualisation methods. In both cases, velocity maps of 2D slices were produced. In the last few years, papers on visualising of flow in extrusion using MRI have been published, especially with regard to the food industry. Agemura et al. (1995) used MRI to compare the flow fields between two different types of screw-extruders. The method commonly used to look at flow in such systems is the time-of-flight method, which detects the displacement of 'tagged' spins between excitation and signal intensity measurement (Callaghan,

1991a). Flow visualisation using MRI is more appropriate for steady state flows (Pope and Yan, 1993), which is not the case with extrusion where convergence is a common phenomena near the die (Harrison et al., 1984; Fielden et al., 1989).

When extruding ceramic pastes, different considerations must be taken into account. Water moves much less freely in ceramic pastes during extrusion, in comparison to the water movement that occurs when extruding most of the pharmaceutical formulations. Furthermore, the extrusion process in the pharmaceutical industry is more complex than in any other industry, because considerations must be taken to ensure that the material has the properties required for both extrusion and spheronisation. Unfortunately, different physical properties are needed for a material to successfully undergo the two-stage process. For example, a material that extrudes well should have appropriate plasticity, whereas a degree of brittleness of the extrudates is required if they are to break on the spheroniser. These chopped length extrudates should be of sufficient plasticity to round to spheres. Using a non-invasive method on the extrudates the distribution of water inside the samples could be mapped without needing to slice the extrudates and by that change the water structure.

1.1. Nuclear magnetic resonance (NMR)

The theory of nuclear magnetic resonance is well known and the reader is referred to several texts on the subject (Callaghan, 1991a), as a detailed discussion is not appropriate here. Briefly however nuclear magnetic resonance occurs when nuclei possessing a magnetic moment, $\boldsymbol{\mu}$ are placed in an external magnetic field, $\mathbf{B_0}$, and irradiated with radio-frequency (RF) radiation, $\mathbf{B_1}$, perpendicular to $\mathbf{B_0}$. Nuclei having a magnetic moment also posses 'spin', a form of angular momentum characterised by the spin quantum number, I, which for the hydrogen nucleus is equal to $\frac{1}{2}$. When a sample containing nuclei with a magnetic moment is placed in a static magnetic field, $\mathbf{B}_0$, (pointing along the laboratory z-axis) the nuclear moments populate themselves between two distinct energy levels. The population difference between these two levels is governed by the Boltzmann distribution (Harris, 1986) and gives rise to a net magnetisation vector $\boldsymbol{M_0} = (\boldsymbol{i}M_x, \boldsymbol{j}M_y, \boldsymbol{k}M_z)$. Transitions between these two energy levels may then be induced by irradiating the system with electromagnetic irradiation whose frequency is proportional to the difference of the energy level spacing:

$$\Delta E = \gamma h \mathbf{B_0} = h\omega_0 \tag{1}$$

Where γ is the gyromagnetic ratio for ^{1}H, h is Planck's constant and ω_0 is known as the Larmor frequency. In modern NMR spectroscopy and imaging a pulse of electromagnetic radiation in the radio frequency (RF) region is used to perturb the distribution of spins between the two energy levels. After the pulse, an RF NMR signal is detected as the equilibrium distribution between the two levels is restored. The time dependence of the signal is then monitored from which a frequency spectrum may be obtained via Fourier transformation. A single sharp line in the frequency domain will result if the sample contains a single proton chemical species, e.g. water.

1.2. Magnetic resonance imaging (MRI)

Spatial resolution is achieved by the superposition of additional smaller magnetic field gradients (usually in the x, y, and z) to the main field $\mathbf{B_0}$. Gradient and RF excitation pulses may then be combined (Callaghan, 1991a) to produce one-two and three-dimensional spatial maps of the spatial spin distribution, more commonly known as the 'spin-density' given by:

$$\rho(\mathbf{r}) = \iiint S(\mathbf{k}) \exp[-i2\pi \mathbf{k}.\mathbf{r}] d\mathbf{k} \tag{2}$$

where $\rho(\boldsymbol{r})$ is the spin density, $S(\boldsymbol{k})$ is the signal, $\boldsymbol{r}$ is the position vector of the spin(s) in the sample and $\boldsymbol{k}$ is defined as the reciprocal space vector (Callaghan, 1991b)

$$\mathbf{k} = (2\pi)^{-1} \gamma \mathbf{G} t \tag{3}$$

and $\boldsymbol{G}$ is the strength (and direction) of the additional magnetic field and t is the time for which $\boldsymbol{G}$ is applied. In this study 3-dimensional volume magnetic resonance imaging was used to

obtain a full 3D spatial map of the spin-density of water protons within the extrudate. The pulse sequence involves the use of a normal spin-echo using pure hard pulses (Callaghan, 1991a) and three orthogonal gradients G_x, G_Y and G_z as shown in Fig. 1(a). This type of sequence has the advantage of minimising the echo time in the experiment, a discussion of which is given below.

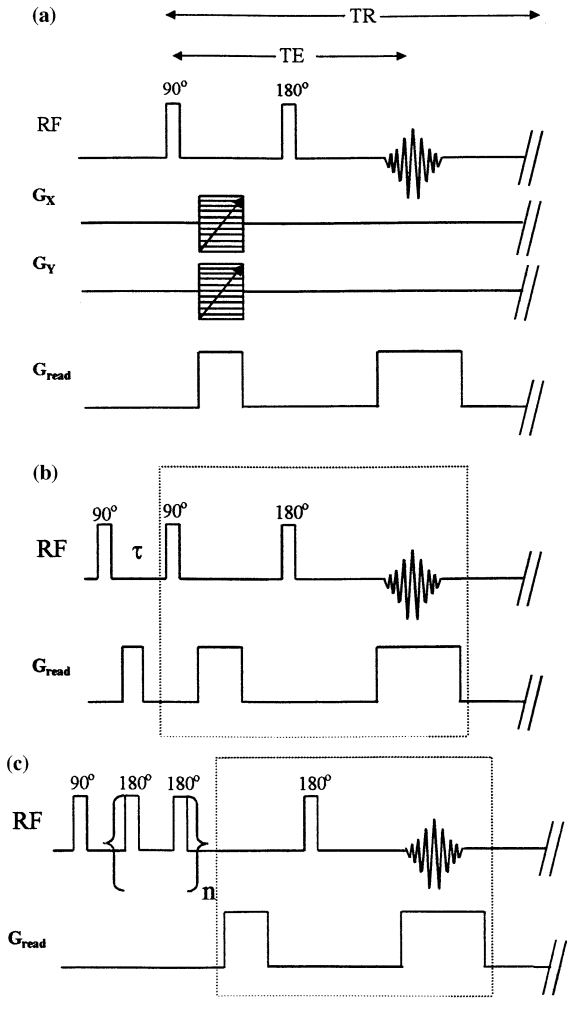

Fig. 1. (a) Schematic of the 3D volume imaging pulse sequence. Here the z-direction is equivalent to the G_{read}. The 'echo time', TE, and 'recycle time' TR are indicated. (b) T_1 profiling pulse sequence. The first 90° pulse is a saturating pulse which is subsequently followed by a variable delay τ. A normal profiling sequence (indicated by the dashed box) is then used to acquire T_1 weighted profiles. (c) T_2 profiling sequence. Here a variable 'echo time' is achieved using a preconditioning train of 'n' 180° pulses (a CPMG train) before the normal profiling sequence (indicated by the dashed box).

1.3. Relaxation processes

The recovery of the equilibrium magnetisation condition following an excitation pulse is governed by two time constants, T_1 and T_2 known as spin-lattice and spin-spin relaxation times, respectively. In liquid like systems (which is the case here) the spin-lattice relaxation time is governed by the following equation:

$$\frac{dM_z}{dt} = -\frac{(M_z - M_0)}{T_1} \tag{4}$$

where M_z is the magnetisation along the z axis, M_0 the equilibrium magnetisation and T_1 is the spin-lattice (or longitudinal) relaxation time. The solution of Eq. (4) is given by:

$$M_z(t) = -M_z(0)[1 - \exp(\frac{-t}{T_1})] \tag{5}$$

where $M_z(0)$ is the magnitude of the z-magnetisation at equilibrium. The 'Lattice' in this case is used as a general term for the nuclear environment. The spin-lattice relaxation process can be also explained as relaxation of the over excited resonating spin system by the transfer of its excess energy to the surrounding thermal reservoir. This flow of energy occurs between the nuclear spin system and the other degrees of freedom in the system, 'lattice'. The spin-lattice relaxation time, T_1, at room temperature is typically in the range of 0.1–10 s for protons.

Thermal equilibrium in the xy plane is described by the time constant T_2, known as the spin-spin relaxation (or transverse) time:

$$\frac{dM_x}{dt} = -\frac{M_x}{T_2} \quad \text{and} \quad \frac{dM_y}{dt} = -\frac{M_y}{T_2} \tag{6}$$

Relaxation of M_x and M_y are caused by direct interactions between the spins of different nuclei. The spin-spin relaxation time, T_2, is usually in the range of 10 μs to 10 s. The relationship between the two time constants is a complex one, though it has been shown that $T_2 \leq T_1$ (Callaghan, 1991c). The two relaxation phenomena, although described by two different time constants, occur

simultaneously. The integrated form of Eq. (6) is as follows:

$$M_{x,y}(t) = M_{x,y}(0)\exp(\frac{-t}{T_2}) \quad (7)$$

This exponential behaviour applies where the interactions responsible for relaxation in the transverse direction are weak. However, for solids undergoing very slow motions the decay is more complicated than this.

T_1 and T_2 processes are of great importance in NMR experiments and when designing an NMR experiment, consideration of their effect should be taken. For example, if the 'recycle delay' (the time between successive RF excitations) is less than five times T_1 then the equilibrium magnetisation will not recover completely along the z-axis resulting in the net magnetisation vector being less than $\boldsymbol{M}_0$. In this case the resulting detected magnetisation will be non-quantitative.

The spin-spin relaxation characteristics should also be taken into consideration, as they determine for how long the xy magnetisation takes to lose phase coherence in the xy plane after the application of the RF pulse. In systems of short T_2, sometimes there is insufficient time to complete the desired pulse sequence resulting in little or no signal being detected.

It is important to realise that what is actually being measured in these experiments is the intensity of the NMR signal at a time TE (the echo time), which is subsequently recycled at a recycle time TR. The intensity of the observed magnetisation generated immediately after the 90° excitation pulse (I_0) is proportional to the proton concentration when the recycle time, TR, is sufficiently long to allow full relaxation of the NMR signal. When TR does not allow complete relaxation, the NMR signal becomes saturated and the intensity of the observed magnetisation generated immediately after successive 90° excitation pulses has intensity I_s, where $I_s < I_0$. Eqs. (7) and (5) may be combined to yield a relative signal intensity for a given recycle time TR and echo time TE:

$$I_{TE} \approx I_0\left[1 - \exp(\frac{-TR}{T_1})\right]\left[\exp(\frac{-TE}{T_2})\right] \quad (8)$$

1.4. Percolation analysis

Percolation analysis is used in this work to quantify the structure of water distribution within the sample. The first step of percolation analysis is to assign each volume element (voxel) within the data matrix to either have a value of 0 or 1 corresponding to the states 'empty' and 'occupied' respectively. This is achieved in practice by binary gating the data matrix at a particular threshold value; the fraction of voxels assigned to each 'empty' or 'occupied' states varies monotonically with the gating level. A cluster is defined as a continuous group of occupied nearest-neighbour voxels, where two voxels are considered nearest neighbours if they have one face in common. At any particular threshold value used to produce the binary gated image, the 3D volume will consist of a (in general large) number of clusters. A percolating cluster is one such cluster which 'spans' the volume, i.e. extends from side of the 3D volume to the opposite side. The percolation threshold (P_c) is the value of the threshold used to form the binary gated data at which a percolating cluster is first formed. Data sets for all samples were normalised in identical fashion to permit quantitative comparison of the percolation threshold between samples. In this paper the percolation threshold is found by determining, using a binary chop algorithm, the threshold level to form the binary 3D image at which a percolating cluster is first formed. The application of image analysis to consider percolation characterisation in MRI data has been presented earlier. General aspects of percolation theory and its uses are described in Stauffer and Aharony (1994) and Sahimi (1994).

2. Materials and methods

Two different esters of gallic acid, methyl-paraben (Nipa Laboratories, Mid Glamorgan, UK) and propyl-paraben (Nipa Laboratories, Mid Glamorgan, UK) were mixed with microcrystalline cellulose (Avicel PH-101, FMC, Cork, Ireland) in the proportion of seven parts to five parts to which water was added (formulation K: 40% of the total mass and formulation Q: 45.45%

of the total mass). The wet mass was extruded using a ram extruder (2.54 cm diameter barrel) fitted with a single-hole die 2 mm in diameter and 8 mm in length (Ovensten and Benbow, 1968) at a speed of 200 mm/min and 20 mm/min, driven by a mechanical press (Lloyds MX-50, Southampton, UK). The die's diameter used was twice the normal in order to get a better resolution. Hence, the length was also doubled in order to keep the radius to length ratio the same. Once a steady-state was formed the extrudates were collected for 3 s for the 200 mm/min extrusion speed and for 30 s for the 20 mm/min speed. A total of five extrudates were randomly picked using a forceps and placed inside a small glass tube, which is hermetically sealed at the bottom and was sealed at the top using a Teflon tape. The first extrudate out of the five taken was analysed within 2 h from extrusion.

All MRI experiments were performed on a Bruker Spectrospin DMX 200 spectrometer operating at a ^{1}H frequency of 199.7 MHz. Samples for MRI were placed in a 5-mm NMR tube and lowered via an air bearing mechanism into a 5-mm saddle coil. Typical pulse parameters were as follows: ^{1}H 90° pulse = 3.5 μs; 180° pulse = 7.0 μs; recycle time = 3.0 s. Spatial resolution was achieved using a three orthogonal axis (x,y,z) shielded gradient system surrounding the sample. For three-dimensional volume imaging a $128 \times 32 \times 32$ data matrix was acquired where the gradient strengths used were: G_z(read) = 23.52 G cm^{-1} and G_{xy}(phase) = 12.25 G cm^{-1} (Fig. 1(a)). The field of view for all 3D-volume imaging was $10 \times 3.5 \times 3.5$ mm yielding a plane pixel resolution of 109 μm. The echo time (TE) was 1.90 ms. One-dimensional profiles were taken before and after a three-dimensional volume image. The first extrudate examined in the series of five had another 1D profile taken at the end of the five experiments to determine if there was significant water loss during the 10 h over which the five experiments took place. T_1 and T_2 profiles were acquired to investigate relaxation heterogeneities over the length of the sample. The pulses sequences to achieve T_1/T_2 profiles, shown in Fig. 1(b) and (c) respectively, are simple modifications of the basic 1D profiling sequence. For T_1 profiles a 90° saturation pulse followed by a homospoil gradient of duration 5 ms and strength 24.5 G cm^{-1} and then a variable delay was used prior to the 1D profile sequence. In this way it is possible to obtain a series of T_1 weighted profiles which may then be fitted to Eq. (5). T_2 profiles were acquired using a CPMG (Carr and Purcell, 1954) pre-conditioning pulse train prior to the 1D profile sequence. Again a series of T_2 weighted profiles were obtained which were subsequently fitted to Eq. (7). Prior to Fourier transformation the 3D data sets were zero filled in the xy dimensions to yield a data matrix size of $(128 \times 64 \times 64)$ and thus an improved albeit smoothed in plane resolution of approximately 55 μm.

Structural analysis of the distribution of water in the sample was performed using a percolation algorithm using in-house image analysis software on a Sun Sparc 20 workstation. The preparation of the samples involved breaking of the extrudates and this produces uneven surfaces at the axial edges of the cylindrical extrudate. For the structural analysis a comparable region of each sample must be considered. This is achieved defining boundaries that are common to all by chopping the data matrix in the z (axial direction) prior to percolation analysis.

3. Results and discussion

The recycle time (TR) used was 3.0 s and the echo time (TE) was 1.9 ms. The relaxation times measured as described above were as followed: $T_1 = 1.80$ s, $T_2 = 26.90$ ms for the 40% water extrudates, and $T_1 = 1.74$ s, $T_2 = 25.81$ ms for the 45% water extrudates. Using these values in Eq. (8), gives that 23.4% of the total magnetisation is lost prior to acquisition in the case of the 40% extrudates, and 25.0% with the 45% extrudates. Relaxation corrections may be neglected in this work because T_1/T_2 analysis of the 1D profiles showed that the relaxation parameters were essentially the same for all samples and were homogeneously distributed across the 1D profile. From examination of the 1D profiles, produced for the first extrudate, examined from each sub-group of extrudates before the experiment and after all the

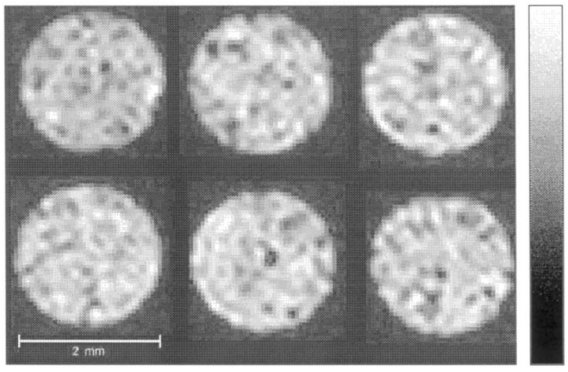

Fig. 2. 2D *xy* slices extracted from the 3D image from an extrudate produced by extruding a mixture of methyl paraben/MCC with 40% water at 200 mm/min. White dots represent the presence of water. Each slice is 78 μm thick and has an in-plane (*xy*) pixel resolution of 55 μm.

five extrudates from its sub-group were analysed, it was found that negligible water loss had occur during this time (1.4%). The comparison between the 1D profile taken before and after the 3D experiment of each extrudate resulted in variation less than 1.4%.

Fig. 2 shows an *xy* ^{1}H spin-density map of an *xy* slice extracted from the 3D data set. In contrast to the obvious water differences that were easily seen from the slices produced from the plug samples, the extrudates were seem to be relatively homogeneous in water contact without any wetter or drier regions. A graph of water intensity as a function of distance along the radial diameter is shown in Fig. 3. The water level in all of the samples was relatively consistent along the diameter without any obvious differences across the slice. This is in contradiction to the expected higher concentration of water near the die wall that would result if water migrated to the circumference.

By increasing the diameter of the die, one is minimising the effects of the die walls. Furthermore, Harrison (1982) showed that at low shear rates the flow inside the die is a Newtonian parabolic flow, where only at high shear rates does the plug flow start to be predominant. Here, again due to the relatively wide die used, the shear rates are relatively low; hence, a parabolic flow can be assumed to occur inside the die. This type of flow would be expected to be much more uniform with respect to water differences in comparison to the plug flow.

When examining the percolation thresholds calculated for the different extrudates, displayed in Table 1, higher values were recorded for the extrudates produced using the slow extrusion speed (20 mm/min) than those produced by extruding at 200 mm/min. Furthermore, higher percolation threshold values were measured for the extrudates

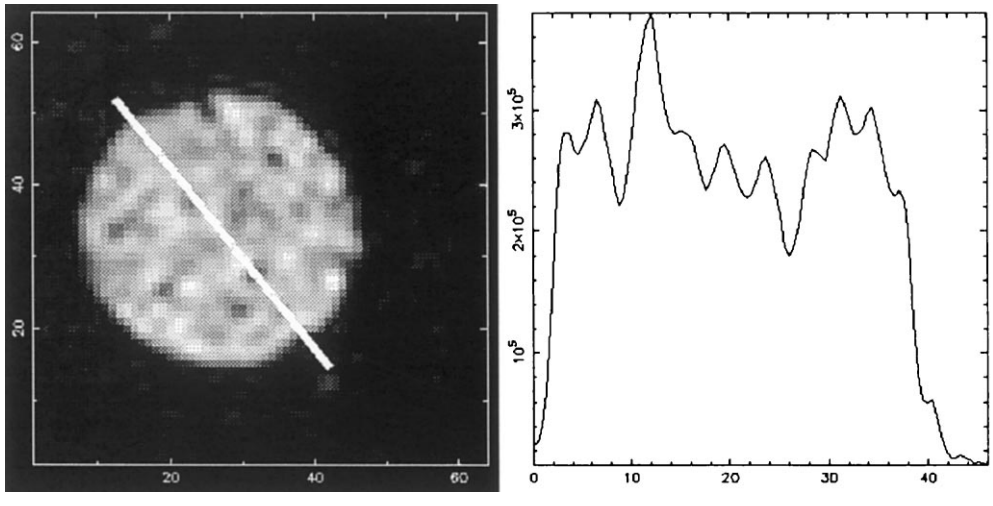

Fig. 3. The graph of water intensities (*y*-axis) as a function of the position (*x*-axis) along the white line marked across the sample (the noise level for this sample is 4.0×10^4).

Table 1
Percolation thresholds averages and coefficient of variation (CV) from results of five different extrudates, and extrusion force recorded for the different formulations

Material	% Water	Extrusion speed	Percolation thresholds, average	Percolation thresholds, CV (%)	Extrusion force (kN)
Methyl paraben	40	20	0.322	3.0	1.20
	40	200	0.291	1.2	3.76
	45	20	0.350	2.5	0.51
	45	200	0.297	8.4	1.33
Propyl paraben	40	20	0.338	2.5	1.03
	40	200	0.268	2.1	2.80
	45	20	0.357	2.6	0.64
	45	200	0.314	0.8	1.22

produced from formulation Q (45.45% water) than for those produced from the formulations containing 40.00% of water. Higher percolation threshold values suggest that the water inside the sample is less structured than water in a sample with lower percolation values. From past work on water distribution in extrudates by way of drying extrudates fractions containing the same drug models (Tomer and Newton, 1999), one would expect extrudates produced from slower extrusion speeds or with more initial water in the formulation to be wetter than extrudates produced at faster extrusion speeds or lower initial water content. Therefore, a link between wetter extrudates and higher percolation threshold values (less water structure) is suggested to exist from these results. An explanation for this relationship could not be suggested at this time. A negative correlation of -0.811 at a level of 0.05 significance was found between the percolation threshold calculated and the extrusion force recorded while producing the extrudates investigated. This implies that the water distribution inside the extrudates was more structured with an increase in the extrusion force. This correlation is logical, because an increase in extrusion force increases the amount of water movement, hence, more paths of water should be found in the extrudate structure. Jerwanska et al. (1995) found that all the air escaped downward, from the die and upward from the gap between the piston and the barrel before reaching the steady-state force. Hence, it is assumed that the structure of the extrudate consists of solid and water, with no air present. Therefore, the finding of different structure within the extrudates implies that different saturated structures exist within the different extrudates. The structure at saturation is therefore influenced by the parameters stated before, i.e. speed and initial water content.

From previous experience with extrusion/spheronisation systems, it is well known that when decreasing extrusion speed and/or increasing initial water content, larger pellets will be created. Hence, when comparing the expected pellet size to the percolation threshold measured, one would expect a correlation between lower percolation threshold and smaller pellets: more experiments should be conducted to establish whether such a correlation exists.

4. Conclusions

The magnetic resonance imaging (MRI) method was demonstrated to be a valuable tool in mapping water distribution. From examination of extrudates, no differences in water distribution was found between the extrudates produced in different speeds and from different water content in the initial formulation, though one would expected to find a higher concentration of water at the circumference of the extrudates due to migration of water to the die walls. However, a difference in the amount of water structure within the extrudates was found, though no explanation could be offered at this time as to the origin of

this change in structure. Nevertheless, this change of structure suggests that different levels of liquid saturation exists. A negative correlation between extrusion force and percolation threshold was found which suggests that higher extrusion force accelerates the paths of water forming inside the extrudate. A possible relationship between percolation threshold and pellet size was suggested.

Acknowledgements

The authors would like to thank Dr Paul Alexander (Department of Physics, University of Cambridge) for his help with the image analysis program. G.T. would like to thank the Overseas Research Students (ORS) scholarship scheme and the Leo Baeck scholarship for their support.

References

Agemura, C.K., Kautenand, R.J., McCarthy, K.L., 1995. Flow fields in straight and tapered screw extruders using magnetic resonance imaging. J. Food Eng. 25, 55–72.

Baert, L., Remon, J.P., Knight, P., Newton, J.M., 1992. A comparison between the extrusion forces and spheres quality of a gravity feed extruder and a ram extruder. Int. J. Pharm. 86, 187–192.

Benbow, J.J., Oxley, E.W., Bridgwater, J., 1987. The extrusion mechanics of pellets — the influence of paste formulation. Chem. Eng. Sci. 42, 2151–2162.

Borgia, G.C., Brancolini, A., Camanzi, A., Maddinelli, G., 1994. Capillary water determination in core plugs: a combined study based on imaging techniques and relaxation analysis. Magn. Reson. Imaging 12, 221–224.

Burbidge, A.S., Bridgewater, J., Saracevic, Z., 1995. Liquid migration in paste extrusion. Trans. IchemE 73, 810–816.

Callaghan, P.T., 1991a. Principles of Nuclear Magnetic Resonance Microscopy. Clarendon Press, Oxford.

Callaghan, P.T., 1991b. Principles of Nuclear Magnetic Resonance Microscopy. Clarendon Press, Oxford, pp. 94–95.

Callaghan, P.T., 1991c. Principles of Nuclear Magnetic Resonance Microscopy. Clarendon Press, Oxford, p. 79.

Carr, H.Y., Purcell, E.M., 1954. Effects of diffusion on free precession in nuclear magnetic resonance experiments. Phys. Rev. 94, 630–638.

Chohan, R.K., Newton, J.M., 1996. Analysis of extrusion of some wet powder masses used in extrusion/spheronization. Int. J. Pharm. 131, 201–207.

Fielden, K.E., Newton, J.M., Rowe, R.C., 1989. The effect of lactose particle size on the extrusion properties of microcrystalline cellulose-lactose mixtures. J. Pharm. Pharmacol. 41, 217–221.

Gotz, J., Buggisch, H., 1993. NMR imaging of pastes in a ram extruder. J. Non-Newtonian Fluid Mech. 49, 251–275.

Gullberg, G.T., Simons, M.A., Wehrli, F.W., Row, D.N.G., 1990. Time-of-flight NMR imaging of plug and laminar flow. SPIE physics and engineering of computerized multidimensional imaging and processing. 671, 314–319.

Harris, R.K., 1986. Nuclear Magnetic Resonance Spectroscopy. Longman, New York, p. 9.

Harrison, P.J., 1982. Extrusion of Wet Powder Masses. PhD Thesis, University of London.

Harrison, P.J., Newton, J.M., Rowe, R.C., 1984. Convergent flow analysis in the extrusion of wet powder masses. J. Pharm. Pharmacol. 36, 796–798.

Harrison, P.J., Newton, J.M., Rowe, R.C., 1985. The characterization of wet powder masses suitable for extrusion/spheronization. J. Pharm. Pharmacol. 37, 686–691.

Harrison, P.J., Newton, J.M., Rowe, R.C., 1987. The application of capillary rheometry to the extrusion of wet powder masses. Int. J. Pharm. 57, 235–242.

Hyde, T.M., Gladden, L.F., Payne, R., 1995a. A nuclear magnetic resonance imaging study of the effect of incorporating a macromolecular drug in poly(glycolic acid-DL-lactic acid). J. Controlled Release 36, 261–275.

Hyde, T.M., Gladden, L.F., Malcolm, M.R., Gao, P., 1995b. Quantitative nuclear magnetic resonance imaging of liquids in swelling polymers. J. Polymer Sci. Part A Polymer Chem. 33, 1795–1806.

Jerwanska, E., Alderborn, G., Newton, J.M., Nyström, C., 1995. The effect of water content on the porosity and liquid and liquid saturation of extruded cylinders. Int. J. Pharm. 121, 65–71.

Kojima, M., Ando, S., Kataoka, K., Hirota, T., Aoyagi, K., Nakagami, H., 1998. Magnetic resonance imaging (MRI) study of swelling and water mobility in micronized low-substituted hydroxypropylcellulose matrix tablets. Chem. Pharm. Bull. 46, 324–328.

Ovensten, A., Benbow, J.J., 1968. Effects of the die geometry on extrusion. Trans. Br. Ceram. Soc. 67, 543–567.

Pope, J.M., Yan, S., 1993. Quantative NMR imaging of flow. Concepts Magn. Reson. 5, 281–302.

Raines, C.L., Newton, J.M., Rowe, R.C., 1990. Extrusion of microcrystalline cellulose formulations. In: Carter, R.E. (Ed.), Rheology of Food, Pharmaceutical and Biological Materials with General Rheology. Elsevier Applied Science, London, pp. 248–257.

Rajabi-Siahboomi, A.R., Bowtell, R.W., Henderson, A., Davis, M.C., Melia, C.D., 1994. Structure and behaviour in hydrophilic matrix sustained release dosage forms: 2. NMR-imaging studies of dimensional changes in the gel layer and core of HPMC tablets undergoing hydration. J. Controlled Release 31, 121–128.

Sahimi, M., 1994. Application of Percolation Theory. Taylor & Francis, London.

Sinton, S.W., Chow, A.W., 1990. NMR imaging for studies of suspension rheology. Paper presented at Society of Rheology, Sante Fe, NM, 21–25 October.

Stauffer, D., Aharony, A., 1994. Introduction to Percolation Theory, 2nd ed. revised. Taylor & Francis, London.

Tomer, G., Newton, J.M., 1999. Water movement evaluation during extrusion of wet powder masses by collecting extrudate fractions. Int. J. Pharm. (in press).

Tomer, G., Newton, J.M., Kinchesh, P., 1999. Magnetic resonance imaging (MRI) as a method to investigate movement of water during the extrusion of pastes. Pharm. Res. 16, 666–671.